ASAXS study of the influence of sulfidation conditions and organic additives on sulfide slabs multiscale organization

Séverine Humbert, Elodie Devers, Clément Lesage, Christele Legens, Laurent Lemaitre, Loic Sorbier, Frédéric de Geuser, Valérie Briois

To cite this version:

Séverine Humbert, Elodie Devers, Clément Lesage, Christele Legens, Laurent Lemaitre, et al.. ASAXS study of the influence of sulfidation conditions and organic additives on sulfide slabs multiscale organization. Journal of Catalysis, 2021, 395, pp.412-424. 10.1016/j.jcat.2021.01.033 . hal-03163091

HAL Id: hal-03163091
https://hal.science/hal-03163091

Submitted on 9 Mar 2021

ASAXS study of the influence of sulfidation conditions and organic additives on sulfide slabs multiscale organization

S. Humbert [a]#, E. Devers [a], C. Lesage [a,b], C. Legens [a], L. Lemaitre [a], L. Sorbier [a], F. De Geuser [c], V. Briois [b]

[a]*IFP Energies nouvelles, Rond-point de l'échangeur de Solaize, BP 3, 69360 Solaize, France*

[b]*SOLEIL Synchrotron , BP48, L'Orme des Merisiers , Gif-Sur-Yvette , 91192 Saint-Aubin, France*

[c]*SIMaP, Grenoble INP, CNRS, Université Grenoble Alpes, 38000 Grenoble, France;*

#corresponding author

severine.humbert@ifpen.fr

Abstract

One of the ways to improve the activity of the sulfide catalysts is to increase the quantity of molybdenum up to contents greater than 15 wt.%. For such high Mo contents, the distribution of MoS_2 particles is suspected to play an important role in the catalytic activity. A complete description of the active phase is thus required and implies measuring i) the size and stacking distribution of the isolated slabs, ii) the proportion of Mo involved in aggregates or individual slabs, iii) the size of the aggregates. These steps are essential to deeply explain the intrinsic activity of the catalysts. To address this challenge, Anomalous Small-Angle X-ray Scattering (ASAXS) analyses have been performed on different sets of catalysts, prepared with various organic additives and activated either by a gas sulfidation (1 bar, 350°C,15%H_2S/H_2) or by real industrial liquid sulfidation (30 bar, 350°C, H_2/gas oil/DMDS). Furthermore, the spent catalysts were also characterized after HDS catalytic test on a real feedstock. The aim of this study was not to elucidate in detail the chemical mechanisms involved when using additives or different sulfidation conditions, but rather to better understand the impact of the microstructural organization on catalytic performances and demonstrate the potential of the ASAXS technique to give new insights on the multi-scale organization of the molybdenum active phase. We thus demonstrate that ASAXS allows to obtain a more detailed description of the slabs compared to TEM and, simultaneously, to identify and quantify the aggregation state of the particles which occurs on high loaded catalysts. The role of the additives is clearly highlighted after liquid sulfidation, as we demonstrate the dispersive effect of triethylene glycol and thioglycolic acid and to a lower extent of citric acid. The slab length and stacking are decreased, as well as the aggregate amount and size. The analysis of the spent catalysts have also revealed the significant evolution of the active phase under HDS reaction conditions. Among other parameters, the aggregate amount appears as a relevant descriptor since a correlation is found with the intrinsic catalytic performances, which suggests an issue of active sites accessibility.

Keywords

ASAXS, CoMoP HDS catalysts, slabs, aggregates, Liquid sulfidation, Gas sulfidation, additives

1 Introduction

The development of more efficient catalysts is today a major challenge to meet the increasingly demanding environmental and economic constraints on chemical processes. Among them, hydrotreatment (HDT) is a key step in the refinery to obtain fuel which complies with the strengthened regulations on their heteroatom content, and particularly on sulfur. Indeed, sulfur compounds are not only generators of SO_x emissions during fuel combustion but are also poisons for catalytic converters [1]. HDT catalysts are composed of a group VI transition metal, like molybdenum or tungsten, promoted by a group IX or X transition metal, such as cobalt or nickel. Dispersed on a porous material, mostly γ-alumina as oxidic phases [2,3] they need to be sulfided using hydrogen and a sulfiding agent to be active for HDT.

The preparation of new and more active hydrotreating catalysts can be performed in two ways: (i) introduction of a larger amount of molybdenum with the same specific activity; (ii) increase of the specific activity per molybdenum. The specific activity (activity per molybdenum atom) can be increased through two routes: by modifying the nature of the support [4] or by using additives such as phosphorus or organic molecule [5] in the preparation of the catalyst. Phosphorus is nowadays generally added, in the form of phosphoric acid, to favor the formation of heteropolyanions (HPA) and improve the oxide precursor distribution at the surface of the support [6]. As for organic additives, they have a different function depending on their nature, since they can act as dispersing [7][8][9] or solvating agents [10][11]. They can prevent the active phase interactions with the support, while limiting the growth of MoS_2 sheets or delay the gas sulfidation of the promoter to obtain a better synergy between Co and Mo and improve the formation of the "CoMoS" active phase.

Despite very active research in the field, the physico-chemical phenomena involved during the activation are not yet fully understood, mainly because of the representativeness of the analyzed sample. Indeed, most of the characterization results reported in the literature are obtained on sulfided catalysts resulting from the so-called gas phase sulfidation carried out under a gaseous mixture of H_2 and H_2S usually at atmospheric pressure. This activation protocol is indeed easier to carry out and faster than the industrial liquid phase sulfidation carried out at high pressure (30 bar) under H_2 and gas oil containing a light organic sulfur compound. However, gas-phase and liquid-phase sulfidation lead to quite different catalytic activities [12] and stabilities: liquid sulfided catalysts have been reported to be less sensitive upon coke deactivation [13]. A difference has been highlighted on the slabs morphology since liquid sulfided catalysts contain more single MoS_2 layers whereas, after H_2S/H_2 gas sulfidation, some MoS_2 stacks appear [10,14]. The main difference lies in the temperature at which sulfidation starts which is ~50°C and around 220°C for gas and liquid sulfidation, respectively. This difference in temperature of sulfur feeding together with very different heating ramps leads to different sulfidation kinetics of Mo and Co for both activation mode [15], involving different number and nature of intermediates species [16].

Finally, to increase the overall activity of the catalysts, a larger quantity of molybdenum is often introduced, leading to high molybdenum contents (above 15 wt.% of Mo). For high Mo contents, the distribution of MoS_2 particles is suspected to play an important role in the catalytic activity. Thus, the dispersion (i.e. the number of active and accessible Mo atoms) and the distribution of the active phase within the catalyst, which depend both on the properties of the additive used for oxidic precursor preparation and the sulfidation conditions, must be fully characterized.

The active phase physico-chemical properties, such as the sulfidation rate, the promotion rate and the slab morphology, are mostly studied at the slab scale. However High Angle Annular Dark Field Scanning Transmission Electron Microscopy (HAADF-STEM) highlights a multi-scale organization of the active phase (as illustrated in Figure 1) by the presence of slabs, eventually stacked, and by a supplementary meso-scale with the presence of slab aggregates of few dozen nanometer size. These slab aggregates are supposed to fill part of the carrier porosity. Yet until now the impact of this microstructural organization on catalytic performances has not been fully understood.

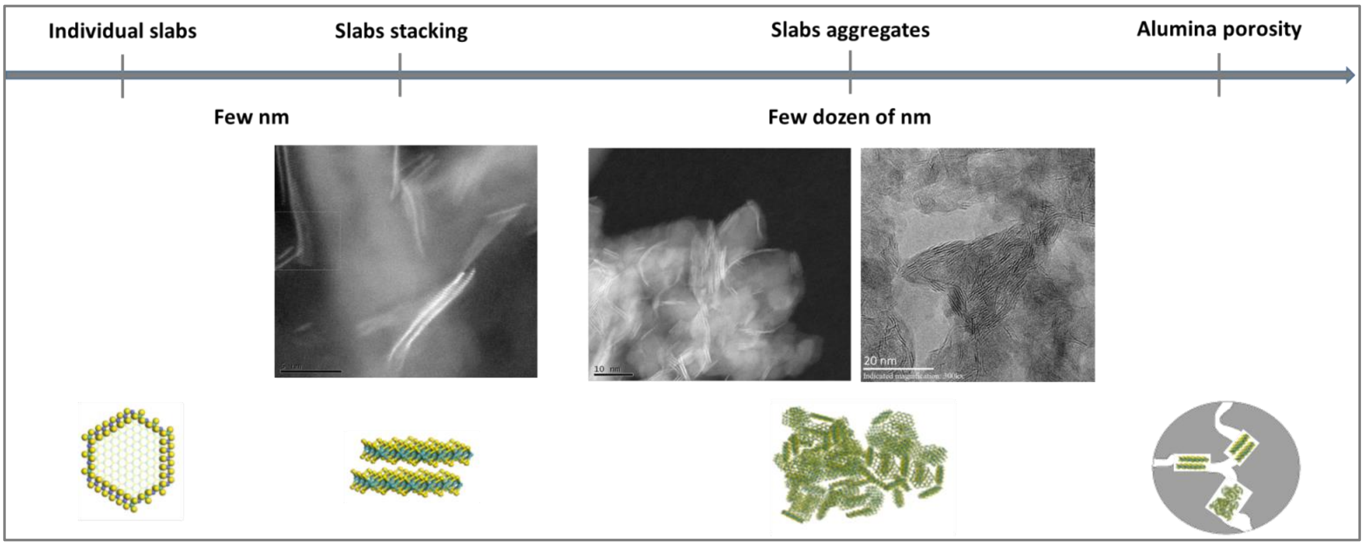

Figure 1. Multi-scale organization of sulfided molybdenum catalysts observed by STEM-HAADF.

For this purpose, a complete description of the active phase implies measuring i) the size distribution of the isolated slabs, ii) the proportion of Mo involved in aggregates or individual slabs, iii) the size of the aggregates. These steps are essential to deeply explain the intrinsic activity of the catalysts.

Several complementary techniques are commonly used to characterize the sulfided catalysts. In particular, the mean slab length and stacking are usually measured by Transmission Electron Microscopy (TEM), the sulfidation and promotion rate can be assessed by X-ray Photoelectron Spectroscopy (XPS) or by Extended X-Ray Absorption Fine Structure (EXAFS). The aggregates can be observed by HAADF-STEM techniques as done on cobalt-based catalysts [17–19] but its use is rarely applied on sulfide catalysts [20].

To address this challenge concerning the multi-scale characterization of the molybdenum sulfided catalysts, Small-Angle X-ray Scattering (SAXS) technique seems particularly effective to study the size distributions of molybdenum particles on supports for many reasons. This technique is only sensitive to electronic density variations and is known to be well-adapted to characterize multi-scale systems as it has already proved its possibilities to characterize the size and morphology of aggregates [21,22]. A variant of this technique is the Anomalous Small Angle X-ray scattering (ASAXS) which allows to target a specific chemical element, Mo in our case. It requires protocols based on numerous controls of the measurement parameters to ensure good control of the uncertainties, which is essential in the case of ASAXS measurement [23], but permit characterizing various sample form such as pellet, powder or liquid without strong experimental constraint. Haubold [24–27], Benedetti [28,29] and Binninger [30] had already demonstrated the ASAXS potential on noble metal particles (Pt or Au) more or less loaded (<1% to 10% by weight of metal) on graphitic matrix. However, ASAXS technique is nowadays seldom used for the characterization of the active phases of catalysts, despite the fact that i) it is well appropriate for a three-phase system (pores, alumina and nanoparticles), ii) it has the advantage of being able to characterize objects with a size between one nanometer and a few hundred nanometers, thus covering the scales of isolated particles and aggregates of particles and iii) it is suitable for high-metal-loaded catalysts. These points have been recently successfully demonstrated on 15%wt cobalt-based catalysts [19].

To our knowledge, this is the first time this technique is implemented to characterize the sulfide slab multiscale organization of CoMoP catalysts. Indeed, van Haandel et al. [31] have used *in situ* SAXS, but without the element sensitivity provided by ASAXS, to study the sulfidation of CoMoS catalysts. They suggested that formation of MoS_2 nanoparticles involved coalescence of small nuclei in close proximity into more elongated structure in one direction, which could be the precursor of the layered MoS_2 structure. Hence, this interesting study only focused on the slab stacking formation. The aim of our study is thus not to elucidate in detail the chemical mechanisms involved when using additives or different sulfidation conditions, but rather to give new insights on the multi-scale organization of the molybdenum active phase, and better understand the impact of this microstructural organization on catalytic performances, depending on the synthesis conditions. We thus propose to study the main trends such as i) the influence of organic additive addition, ii) the influence of the sulfidation conditions (liquid and gas sulfidation) on the Mo repartition, iii) the evolution of the slabs under catalytic reaction conditions and finally iv) the influence of the slab aggregation on the intrinsic activity.

Indeed, these differences in operating conditions of the activation step can impact the sulfidation mechanism of the metallic phase and the morphology of the MoS_2 slabs as shown in different studies [10,14–16,32]. But the impact of the activation process and of the use of additives on the organization of MoS_2 slabs at a higher scale than few nanometers is generally not studied, although it can impact the accessibility of molecules to be desulfurized and thus the catalytic performance. This is what we propose to study in this paper.

2 Experimental

2.1 Catalysts preparation

A series of $CoMoP/Al_2O_3$ catalysts were synthesized by incipient wetness impregnation of γ-alumina extrudates (surface area 270 m^2/g, porous volume 0.77 mL/g) with a solution of MoO_3 (sigma-Aldrich, purity: 99.93%), $Co(OH)_2$ (sigma-Aldrich, purity: 96.21%), H_3PO_4 (sigma-Aldrich, purity: 85%) and distilled water. The target amount of MoO_3 on the final catalysts was 22 wt.% and the Co/Mo and P/Mo molar ratios were 0.4 and 0.55, respectively. Additives such as citric acid (CA), triethylene glycol (TEG) and thioglycolic acid (TGA) were co-impregnated by dissolution in the solution containing the metallic precursors or post-additivated. The molar ratio additive/Mo was between 0.4 and 0.5, except for TGA which due to the solution viscosity was limited to 0.2. The catalysts were maturated in a saturated water atmosphere at room temperature (RT) for 24 h and finally dried under air at 120°C for 6 hours. The non-additivated CoMoP catalyst was also calcined by heat treatment under air (110 L/h/g) with a ramp of 5°C/min up to 550°C for 2 hours. The objective was clearly to obtain catalysts with different aggregation properties. This is why the nature of the additives, as well as the method of additivation and the sulfidation techniques described below, have been varied.

2.2 Sulfidation of catalysts

For the study, the oxide catalysts were activated in two ways. The gas-phase sulfidation, usually performed in the laboratory for practical reasons, consists of using a 15% H_2S/H_2 mixture with a flow rate of 10 L/h/g of catalyst, from RT to 400°C at 2°C/min and under atmospheric pressure. This step is followed with a 2-hour plateau at 400°C under the same gaseous atmosphere, then the temperature is decreased to RT and the gas switched to N_2. The samples are then kept under vacuum in glass sealed cells. They are named herein with “-gas” extension (Table 2).

At the industrial level, the sulfidation step is carried out using a gas-liquid phase with H_2, gas oil spiked with light organic compound containing sulfur such as dimethyldisulfide (DMDS), at high pressure (30 bar) and 350°C. These conditions are applied to the series of oxide catalysts with a first temperature ramp from RT to 190°C at 0.4°C/min and then slowed to 0.2°C/min until 350°C, followed by a 8-hour plateau. During the sulfidation, the H_2 flow and the liquid flow are set, respectively at 5 L/h and 0.02 L/h to keep a liquid hourly space velocity (LHSV) at 1 h^{-1} (volume of catalyst to be sulfide : 20 mL) and a H_2/hydrocarbon (H_2/HC) ratio of 250. At the end of the sulfidation, the temperature is dropped to 200°C and the pressure to 20 bar to be able to wash the catalyst with toluene for 3 hours under N_2. Finally, the catalyst is dried at 200°C and at atmospheric pressure under N_2 for one night (about 14 hours). It is then unloaded into an argon glove bag before being transferred to a glove box to be stored away from the air. The as-prepared samples are identified herein with “-liquid” extension (Table 2).

The liquid activation takes about 30 hours and the beginning of massive sulfidation generally takes place around 220°C at the decomposition temperature of the sulfur-containing compound added in the gas oil charge [32,33]. This slow procedure is necessary to avoid thermal runaways that can occur during liquid sulfidation. The gas sulfidation lasts only a few hours at atmospheric pressure, with a direct supply of H_2S at RT and heating at a constant rate which is 5 to 10 times faster than for liquid sulfidation.

2.3 Catalytic tests

2.3.1 Hydrogenation of Toluene

The catalytic performances were evaluated in toluene hydrogenation (HYD) reaction using a fixed bed unit reactor Flowrence (from Avantium) that contains 16 parallel reactors. Each reactor was filled with 450 µL of the sulfide (either gas or liquid activated as described above) catalyst diluted in Zirblast®. To avoid the oxidation of the catalyst, the reactors have been filled in a glove box. The feed was composed of dimethyldisulfide (DMDS, 5.8 wt%) and toluene (20 wt%) in cyclohexane (74.2 wt%). The hydrogen to feed ratio (H_2/HC) was 450 NL/L and the total pressure 60 bar. The temperature was increased from RT to 350°C with a ramp of 2°C/min and a LHSV of 4 h^{-1}. When 350°C was reached, LHSV was turned down to 2 h^{-1}. The liquid products of the reaction at different temperatures were analyzed by gas chromatography using a DB1 column. The first-order rate constant (k, h^{-1}) was calculated by the following expression (1):

$$k = LHSV * \ln\left(\frac{1}{1-x}\right), LHSV = \frac{flow\ rate\ of\ the\ feed}{volume\ of\ the\ catalyst}, k' = \frac{k}{gMoO3/mL} \qquad (1)$$

x is the percentage conversion of toluene (HYD) in the feed. $LHSV$ is the liquid hourly space velocity (h^{-1}). The intrinsic rate constant k' (cm^3/g(Mo)/h) is obtained by normalizing k with the mass of MoO_3 loaded in the reactor.

All the catalytic results will then be expressed as the Relative Intrinsic Activity $RIA(HYD)$, the dried catalyst activity being the reference, according to equation (2).

$$RIA(HYD) = \frac{k'catalyst}{k'dried\ catalyst} \qquad (2)$$

2.3.2 Hydrotreating of gas-oil feed

The catalysts were also tested in hydrodesulfurization (HDS) of a mixture of straight-run gas oil (SRGO) and light cycle oil (LCO) containing 6815 ppm of S and 488 ppm of N. The density of the feed mixture at 15°C was 0.8795 g/mL. The test was carried out in an isothermal fixed bed reactor. First, *in-situ* sulfidation of the catalysts was performed at 350°C and 40 bar pressure using a SRGO feed with 2 wt% of DMDS added. Then the HDS test was performed during 150 h under the following operating conditions: a total pressure of 40 bar, a catalyst volume of 480 µL, a temperature of 330°C, a hydrogen flow rate of 2.56 mL/min, and a feed flow rate of 0.48 mL/h (LHSV = 1 h^{-1}).

The S content (in ppm) in the effluents was analyzed by X-ray fluorescence (ASTM D4629-2002). The rate constant of HDS reaction (k, h^{-1}) was calculated by using the power rate law with the following expression (3):

$$k = \frac{LHSV}{n-1} * \left(\frac{1}{A^{(n-1)}} - \frac{1}{{A_0}^{(n-1)}}\right), n = 1.3, k' = \frac{k}{gMoO3/mL} \qquad (3)$$

$$RIA(HDS) = \frac{k'catalyst}{k'dried\ catalyst} \qquad (4)$$

A_0 and A represent the sulfur contents at the inlet and the outlet of the reactor, respectively. n is the apparent order versus S and 1.3 is the typically observed order for HDS processes of gas-oil feeds that contain mixture of different sulfur compounds [34]. As previously described, k is normalized by the mass of loaded Mo in the reactor to obtain k'. As for the hydrogenation activity, the results will be expressed as the Relative Intrinsic Activity (RIA), the dried catalyst being the reference catalyst as given by expression (4).

The used catalysts have been recovered after the catalytic test using real feedstock to be further characterized. They are named hereafter with “-spent” extension.

2.4 Characterization techniques

2.4.1 Transmission Electron Microscopy (TEM)

The sulfided catalysts were characterized by Transmission Electron Microscopy. Measurements were carried out in bright field mode with a FEG TECNAI TEM operating at 200 keV. The catalysts were removed from their sealed container, crushed, diluted in ethanol and deposited on a holey carbon copper grid. Ethanol was then evaporated before TEM analysis was performed. The distribution profiles of the slab size and stacking were obtained by measuring around 200 stacked slabs. The average values were calculated by fitting the histograms with a log-normal distribution. The MoS_2 slabs with a size below 1 nm are not detected.

2.4.2 X-ray photoelectron spectroscopy (XPS)

The XPS sampling of the sulfided catalysts was performed in a glove box under an argon atmosphere, with controlled oxygen and water levels (less than 20 ppm) to avoid their partial reoxidation. The samples were crushed and pressed onto an indium foil that was attached to the sample holder via a double-sided carbon tape. The sample holder was then moved directly to the analysis chamber thanks to the special connection of the glove box to the XPS spectrometer. The XPS spectra were recorded on a KRATOS

AXIS Supra instrument with Al monochromator source (1486.6 eV), a hemispherical analyser operating at fixed pass energy of 20 eV and a delay line detector. The measurements were made at RT in steps of 0.1 eV for molybdenum and aluminium, and at a pressure lower than $5 \cdot 10^{-9}$ Torr in the analysis chamber. Binding energies (BE) of the various elements were referenced to the C 1s level of the contamination carbon at 284.6 eV. The curves were integrated by applying a Shirley-type baseline. The collected spectra were analyzed by using Vision software. The Mo/Al atomic ratio was obtained from the measurement of the corresponding peak area and the use of relative sensitivity factors (RSF), specific to the spectrometer and furnished by the manufacturer. Three different analysis points were measured for each catalyst and the data presented correspond to their average value. The relative error is estimated to be ±10%.

2.4.3 Anomalous small angle X-ray scattering (ASAXS)

Measurements

For ASAXS experiments, the extrudates were crushed and introduced in quartz capillaries of 1.5 mm-diameter, in a glove box.

Anomalous small-angle X-ray scattering experiments have been performed on the D2AM beamline [35] at the ESRF synchrotron. The scattered intensity was measured at three different energies (see Table 1) 19700, 19940 and 19990 eV, slightly below the molybdenum K absorption edge. The incident beam energy has been calibrated with a metallic molybdenum foil. To cover the largest q range, two sample-detector distances (348 mm and 2865 mm) have been selected.

The scattering images were recorded using a XPAD detector. The acquisition time depended on the configuration and was chosen in order not to saturate the detector.

Data reduction

For 1D reduction, raw data were corrected from the scattering of the empty capillary (measured in each configuration) and normalized by the incoming photon flux, transmission and true thickness calculated from the transmission coefficient.

To calibrate the intensity in absolute units, i.e. expressed as differential scattering cross-section per unit volume in cm^{-1}, a glassy carbon, was measured at each energy and each sample-detector configuration. A correction factor has been calculated from the ratio between the NIST data [36] and the experimental data.

Theoretical aspects

For the case of randomly oriented particles with identical shape and size parameterized by R dispersed in a homogeneous matrix, the scattered intensity is given by:

$$I(q) = \frac{N_p}{V_s} \Delta\rho^2 \int_0^\infty P(R)V(R)^2F(q,R)^2\Psi(q,R)\mathrm{d}R \qquad (5)$$

with N_p the number of particles, V_s the sample volume, $\Delta\rho^2$ the contrast factor such as:

$$\Delta\rho^2 = \left(\rho_p - \rho_m\right)^2 \qquad (6)$$

ρ_p and ρ_m the scattering length densities of the particles and the matrix:

$$\rho = r_e \sum_j n_j f_j \qquad (7)$$

n_j the number density of the atom j in the matrix and in the particles, f_j the atomic form factors and r_e the classical Thomson radius (r_e = 0.282 10^{-12} cm).

$P(R)$ is the size distribution function, $F(q,R)$ is the form factor and $\Psi(q,R)$ is the structure factor. This latter one depends on concentration and object sizes and has to be taken into account when particles sizes and distances between them are similar. In our case, interference is sometimes observed at large q because of slab stacking but at smaller q, the objects are enough spaced and well-dispersed so that the structure factor can be considered equal to 1.

However, in the case of metal particles supported on a porous alumina support, the SAXS analysis recorded at only one energy is not sufficient to distinguish the nanoparticles as the porous support also contributes significantly to the signal because of the scattering of the pores. Hence, to isolate the signal specific for each phase, it is therefore mandatory to vary the energy of the incident beam and to perform the measurements near and far from the metal (molybdenum in our case) absorption edge.

It is recalled that the atomic form factor of a species j can be written:

$$f_j(E) = f_0 + f_j'(E) + if_j''(E) \qquad (8)$$

with $f_0 = Z$, the atomic number.

The values of Mo $f_j'(E)$ and $f_j''(E)$ near the Mo K absorption edge (located at 20000 eV [37]) are indicated in the Table 1.

Table 1. Energy-dependent parts of the atomic scattering factor f’ and f” [38,39], near the Mo K-absorption edge (20000 eV).

	Energy (eV)	f’	f”
E_1	**19700**	**-3.550**	**0.552**
E_2	**19940**	**-5.105**	**0.556**
E_3	**19990**	**-6.934**	**0.761**

Tuning the energy allows to vary the scattering length density of the molybdenum particle without varying the one of the porous support. The interest of ASAXS analysis, compared to classical SAXS is demonstrated in supplementary information.

Two kind of method can be performed to extract the ASAXS signal of the metallic particles. Lot of authors had used the subtraction method [24–28,40]. It consists in subtracting the intensities measured at two different energies and to use the resulting intensity as a function of the particles scattering. The second method consists in decomposing the total scattered intensity in three components [41–44]: the independent normal SAXS, a cross-term related to the interaction between the particles and the support, and the pure resonant scattering term only due to the particles. Both methods were investigated and are compared in supplementary information.

In this work, the subtraction method was used, taking into account the contribution of the scattering interferences between catalyst particles and the alumina support, such as:

$$\langle I(q,E_i)\rangle - \langle I(q,E_j)\rangle = n_p^2 r_e^2 \left(\left|f_p(E_i)\right|^2 - \left|f_p(E_j)\right|^2\right) S_{pp}(q) + 2 f_s \left(f_p(E_i) - f_p(E_j)\right) n_p n_s r_e^2 S_{sp}(q)$$

$$= n_p^2 r_e^2 \left(\left|f_p(E_i)\right|^2 - \left|f_p(E_j)\right|^2\right).\left(S_{pp} + \alpha S_{sp}\right) \qquad (9)$$

where $\overline{f_p} = \frac{f_p(E_i)+f_p(E_j)}{2}$ is the mean value of $f_p(E)$ and $\alpha = \frac{n_s\, f_s}{n_p\, \overline{f_p}}$

$$S_{pp}(q) = \frac{N_p}{V_s} \int_0^{+\infty} P_p(R_p) V_p^2(R_p)\, F_p^2(q,R_p)\, \mathrm{d}R_p \qquad (10)$$

$$S_{sp} = \frac{N_p}{V_s} \iint_0^{\infty} P_p(R_p) P_s(R_s) V_p(R_p) V_s(R_s) F_p(q,R_p) F_s(q,R_s) \frac{\sin\left(q(R_p+R_s)\right)}{q(R_p+R_s)}\, \mathrm{d}R_p \mathrm{d}R_s \qquad (11)$$

with n_p the number density of the atoms in the particles, f_p the atomic form factor and r_e the classical Thomson radius ($r_e = 0.282\ 10^{-12}$ cm), as defined previously in literature [24–26,40].

Data modeling

To evaluate the size distribution of the sulfide slabs, a nonlinear least-squares adjustment of the ASAXS I(E_1) – I(E_3) curves is performed on equation (9). The assumptions made for the choice of the regression model are listed below.

Given the shape of the curves (two inflections of the scattered signal), two kinds of molybdenum objects have to be considered. Based on the electron microscopy observations, these two populations can be attributed to isolated slab stacks at the small scale, and to larger, polycrystalline and moderately dense slab aggregates at larger scale (see Figure 1).

- Stacked slabs can be modeled as discs of height $2H$ and radius R_p with form factor $F_{disc}\left(q, R_p, H\right)$ and volume $V_p\left(R_p, H\right)$.
- Slab aggregates can be modeled as ellipsoids of revolution (a spheroid) of axes (R_a, R_a and νR_a) with form factor $F_{ellipsoid}(q, R_a, \upsilon)$ and volume $V_a(R_a, \upsilon)$.
- Size distributions of slabs and aggregates are represented by log-normal distributions:

$$P_k(R_k) = \frac{1}{\sqrt{2\pi} R_k \sigma_k} \exp\left(-\frac{(\ln R_k - \mu_k)^2}{2\sigma_k^2}\right) \qquad (12)$$

Where k equals to p for slab stacks and equals to a for the aggregates, and μ and σ are respectively the scale and the shape parameters of the lognormal law.

The size distribution of slab stacks modeled by discs concerns only the radius dimension R_p (the thickness $2H$ is monodisperse), and the size distribution of slab aggregates modeled by a spheroid concerns only the axes R_a (ν takes a single value, so the aspect ratio is fixed).

The number and volume average sizes can thus be calculated from the adjusted log-normal distribution.

To calculate the interference term S_{sp}, the porous support scattering has been modeled thanks to a spherical form factor $F_s(q, R_s)$, a particle volume $V_s(R_s)$ and a bimodal lognormal distribution $P_s(R_s)$ (see. S.I).

The final model reads (see S.I):

$$\langle I(q, E_i)\rangle - \langle I\left(q, E_j\right)\rangle = w_{\mathrm{Mo_x}} \times w_p \times \frac{\rho_s}{\rho_{\mathrm{Mo_x}}} \times \Delta^2_{\mathrm{Mo_x}}\left(E_i, E_j\right) \times \left(S'_{pp} + \alpha S'_{sp}\right) \quad (13)$$

with

$$\Delta^2_{\mathrm{Mo_x}}\left(E_i, E_j\right) = {r_e}^2 \times \left[\left(n_{\mathrm{Mo_x}} f_{Mox}(E_i)\right)^2 - \left(n_{\mathrm{Mo_x}} f_{\mathrm{Mo_x}}\left(E_j\right)\right)^2\right] \qquad (14)$$

$$S'_{pp}(q) = \left[\frac{1}{< V_p >}\int_0^{+\infty} P_p(R_p)\ V_p^2(R_p, H) F_{disc}^2(q, R_p, H) \mathrm{d}R_p + \frac{w_a(1-\varepsilon_a)}{w_p} \right.$$

$$\left. \times \frac{1}{< V_a >}\int_0^{+\infty} P_a(R_a) V_a^2(R_a, \nu) F_{ellipsoid}^2(q, R_a, \nu)\ \mathrm{d}R_a \right]$$

(15)

and

$$S'_{sp}(q) = \left[\frac{1}{<V_p>}\iint_0^{\infty} P_s(R_s) V_s(R_s) F_s(q, R_s) P_p(R_p) V_p(R_p, H) F_{disc}(q, R_p, H)\frac{sin\left(q(R_p+R_s)\right)}{q(R_p+R_s)}\mathrm{d}R_p \mathrm{d}R_s + \frac{w_a(1-\varepsilon_a)}{w_p} \times \right.$$

$$\left. \frac{1}{<V_a>}\iint_0^{\infty} P_s(R_s) V_s(R_s) F_s(q, R_s) P_a(R_a) V_a(R_a, \nu) F_{ellipsoid}(q, R_a, \nu)\frac{sin(q(R_a+R_s))}{q(R_a+R_s)}\mathrm{d}R_a \mathrm{d}R_s \right] \quad (16)$$

with $\mathrm{Mo_x} = \mathrm{MoS_2}$ in the case of sulfide molybdenum and $\mathrm{Mo_x} = \mathrm{MoO_y}$ in the case of oxide molybdenum, $\rho_{\mathrm{Mo_x}}$ the density in g/cm^3 of the molybdenum phase. w_p and w_a are respectively the molybdenum fraction in slabs and aggregates, $w_{\mathrm{Mo_x}}$ the weight concentration of the molybdenum phase (wt.%) and ρ_s the sample structural density in g/cm^3. $< V_p >$ and $< V_a >$ are the mean volumes of respectively slabs and aggregates that may be calculated from the moments of the corresponding log-normal laws (see S.I.).

An example of fit is reported in S.I. This model allows estimating several physico-chemical characteristics. In particular, two parameters can be used to describe the slabs:

- The mean length (in number) $\boldsymbol{L_{slabs}}$ such as :

$$L_{slabs} = 2 \times R_{pnum} \quad (17)$$

- The stacking state $\boldsymbol{z_{slabs}}$ such as :

$$z_{slabs} = \frac{2H}{3.1} \quad (18)$$

3.1 Å being the thickness of one slab according to crystallography [45]. Hence, $z = 1$ when it is a mono-slab and $z = 3$ for a two-stack slabs. The number averaged length is considered here so that it could be easily compared to the mean length measured in TEM.

Three parameters are useful to describe the slab aggregates:

- The aggregate mean width $\boldsymbol{W_{ag}}$ such as :

$$W_{ag} = 2 \times R_{avol} \quad (19)$$

- The aggregate mean length $\boldsymbol{L_{ag}}$ such as :

$$L_{ag} = 2 \times \upsilon \times R_{avol} \quad (20)$$

This aggregate length is however subject to significant uncertainties (see S.I) so that it should not be considered for the comparison of the different samples because of its lack of accuracy.

- The parameter $\boldsymbol{C_{ag}}$ such as :

$$w\mathcal{E} = \frac{w_a(1-\varepsilon_a)}{w_p} \text{ and } C_{ag} = \frac{w\mathcal{E}}{1+w\mathcal{E}} \qquad (21)$$

This parameter traduces roughly the aggregate content (in percent): the higher C_{ag} is, the more aggregated the slabs are, and so the lower the dispersion is.

3 Results and discussion

3.1 Catalyst characterizations

Table 2 summarizes the main characteristics of the sulfided CoMoP catalysts studied herein, using TEM and XPS. Regarding the morphology observed by TEM, it can be shown that average mean slab lengths are roughly the same for the sulfided catalysts in liquid conditions and after catalytic test (~3.4 nm), whereas gas phase activation slightly increases this value to about 4.2 nm, probably due to the higher activation temperature of 400°C used in this protocol. The stacking number is not affected by the different activation treatments and is generally close to 2. Concerning the sulfidation of molybdenum determined by XPS, about 75% is converted into MoS_2 after the activation processes in a liquid or gaseous environment. However, after real feedstock catalytic test, XPS measurements indicate a higher level of sulfidation close to 80% which traduces that the catalysts are still evolving during the test and confirm the interest to characterize them at different steps of their life. If we then focus on the repartition of molybdenum on the alumina surface with the Mo/Al ratio measured by XPS upon liquid sulfidation, we can underline the dispersing role of TEG and TGA additives compared to the dried catalysts as this ratio is increased. After real feedstock catalytic test, TEG catalyst maintains a high dispersion but TGA sample shows a lower dispersion. The calcined or CA additivated catalysts are similar in Mo/Al ratio and higher compared to the dried catalyst, after liquid activation or real feedstock catalytic test, but this ratio is not as impacted as with the aforementioned additives. A much lower metallic repartition is obtained after the gas sulfidation when citric acid is used, whereas TEG improves it as after liquid sulfidation. These numbers will be commented in more details in the next parts when compared with ASAXS results.

Table 2 : TEM and XPS characterizations of the sulfide CoMoP catalysts

		TEM		XPS	
Sample	**Treatment**	**Slabs mean length [nm]**	**Average stacking**	**(Mo/Al)wt.**	**%MoS$_2$**
Dried-liquid	Liquid sulfidation	2.9	1.9	0.33	74.8
Calcined-liquid		3.9	2.0	0.39	69.0
CA-liquid		3.6	1.7	0.38	78.9
TEG-liquid		3.4	1.8	0.52	74.2
TGA-liquid		3.5	1.9	0.43	73.7
Dried-spent	After real feedstock catalytic test	3.6	1.9	0.32	81.1
Calcined-spent		3.5	2.0	0.37	75.4
CA-spent		3.7	1.8	0.37	81.6
TEG-spent		3.3	2.0	0.45	81.4
TGA-spent		3.3	1.7	0.30	79.9
Dried-gas	Gas sulfidation	4.2	2.0	0.32	74.7
CA-gas		4.0	1.8	0.28	75.0
TEG-gas		4.1	2.0	0.40	74.7

3.2 ASAXS deeper characterization

ASAXS curves obtained from the gas sulfided catalysts, liquid sulfided catalysts and spent catalysts are respectively plotted in Figure 2, Figure 3 and Figure 4. After gas phase sulfidation, the scattering curves are quite similar except when citric acid is used as an additive. The liquid sulfidation induces more changes in the shape of the ASAXS curves for the dried catalyst, while for the others a small difference in the separation of the two size ranges exists. Then after real feedstock catalytic test, the difference in molybdenum distribution between all catalyst is more pronounced. Accordingly, these differences in the shape of ASAXS curves give rise to different structural parameters. These parameters, obtained by fitting the curves with the model described above are reported in Table 3.

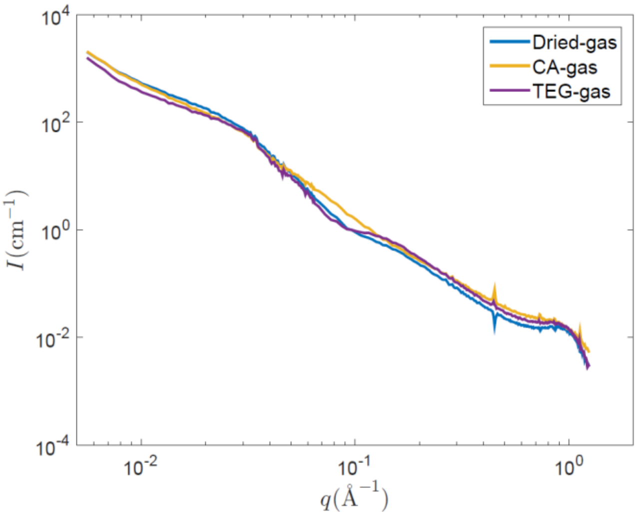

Figure 2. ASAXS curves obtained from the subtraction I(E_1)-I(E_3) on gas sulfided catalysts

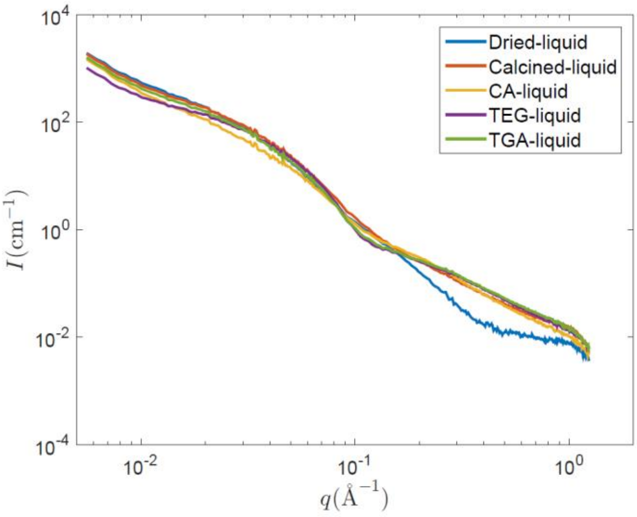

Figure 3. ASAXS curves obtained from the subtraction I(E_1)-I(E_3) on liquid sulfided catalysts

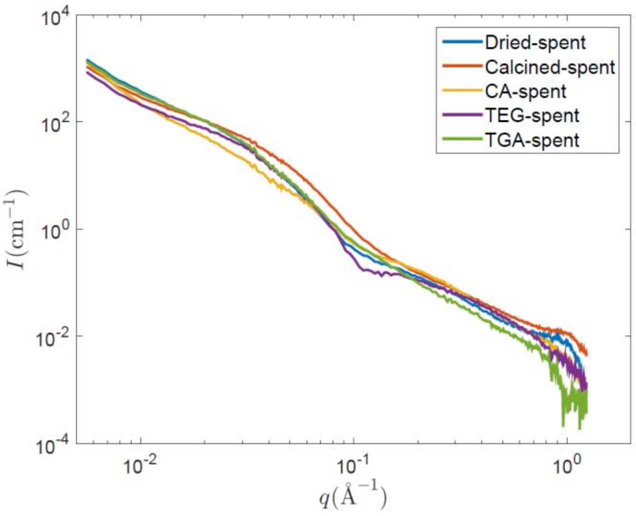

Figure 4. ASAXS curves obtained from the subtraction I(E_1)-I(E_3) on liquid sulfided catalysts after catalytic test

Table 3. Results obtained by fitting the ASAXS curves with the multi-scale model. *The L_{ag} value is subject to significant uncertainties.

Sample	z_{slabs}	L_{slabs} (nm)	C_{ag} (%)	W_{ag} (nm)	L_{ag} (nm)*
Dried-liquid	2.6	4.8	70%	9.9	65
Calcined-liquid	1.0	2.2	31%	9.1	66
CA-liquid	1.9	3.1	33%	10.0	100
TEG-liquid	1.0	1.7	18%	9.1	91
TGA-liquid	1.3	1.7	23%	10.9	86
Dried-spent	1.4	3.1	32%	13.7	109
Calcined-spent	1.3	1.3	34%	9.2	87
CA-spent	2.0	2.5	17%	16.5	165
TEG-spent	1.0	1.8	15%	12.6	125
TGA-spent	1.0	4.7	28%	12.2	92
Dried-gas	2.9	4.1	49%	13.0	130
CA-gas	2.1	5.9	34%	17.4	18
TEG-gas	2.8	4.9	32%	13.2	47

3.2.1 Influence of the additives using liquid sulfidation

Additives appear to have different effects on catalyst activated by liquid sulfidation, in comparison to the dried catalyst (see Figure 3).

The slab length (L_{slabs}) varies from 4.8 to 1.7 nm whereas the slab stacking parameters (z_{slabs}) varies from 2.6 to 1 which correspond to real slab stacking inferior to 2, as explained in section 2.4.3. TEM reports average slab lengths often higher (from 3.4 nm to 3.9 nm) than those determined from ASAXS (between 1.7 and 3.1 nm), except for the dried catalyst which could be suspected to be less well sulfided when analysed in ASAXS. Besides, the slab stacking measured by TEM remains quite constant, around 2. Several reasons can be invoked to explain these differences: i) the small slabs, of the order of 1 nm are difficult to be observed by TEM and ii) the slabs belonging to aggregates can be taken into account during TEM analysis.

For all these reasons, it appears that ASAXS analysis allows one to obtain a more detailed description of the slabs and allows for underlying slight differences between catalysts contrary to TEM analysis.

Based on ASAXS results, it can be noticed that additives have a significant effect on the slab morphology (see Figure 5 A and B): the slab length (L_{slabs}) as well as their stacking (z_{slabs}) decrease when using an additive compared to the dried catalyst, whatever the additive is, but not to the same extent.

TEG and TGA are very efficient, more than citric acid. Additives of glycol-type such as TEG are known to be dispersing agents at the preparation stage [7], leading to an improvement of catalytic activity compared to the dried catalysts irrespective of the activation conditions [8]. But these new ASAXS results confirm that TEG keeps its dispersing properties even after a liquid activation under high pressure and temperature [46]. Citric acid is known to be a complexing agent for oxidic species and its impact on the active phase is more related to an increase of the promotion of MoS_2 slabs [47–51] than the dispersion improvement [52], using gas sulfidation. The reason for such an improvement is associated with the postponing of cobalt sulfidation compared to the dried catalyst at a temperature at which molybdenum is transformed into MoS_2 [50]. Using both citric acid and liquid sulfidation, as we did here, could thus lead to an improvement of the dispersion of molybdenum species, as suggested by Gonzalez-Cortes [53].

At the aggregate scale, the additives have a significant effect on the aggregate content (C_{ag}), as seen in Figure 5-D: it decreases from 70% to 33%, 18% and 23% respectively for the dried-liquid, CA-liquid, TEG-liquid and TGA-liquid samples. These results are confirmed by XPS data: the Mo/Al ratio increases (from 0.33 to 0.52, as shown in Table 2) when using additives, which reveals a higher Mo distribution on the surface, particularly when TEG is used.

The aggregate morphology, quantified by W_{ag} (Figure 5-C) and L_{ag}, is slightly modified as the width varies from 9.9 nm for the dried-liquid to 9.1 nm for the TEG-liquid sample or to 10.9 nm for the TGA-liquid sample. However, the modification remains very minor: the aggregates remain ellipsoidal, relatively thin, around 10 nm-thick and long, with a length higher than 60 nm (Table 3). Hence, it can be assumed that the aggregate morphology of these liquid sulfided catalysts is certainly more oriented by the alumina pore geometry rather than by the additives since they have been prepared on the same carrier.

Based on all these observations, we can conclude that all the additives have a dispersant effect on the molybdenum using liquid sulfidation: the slabs are smaller, less stacked, and better distributed within the support (fewer aggregates), the impact of citric acid being nevertheless lower.

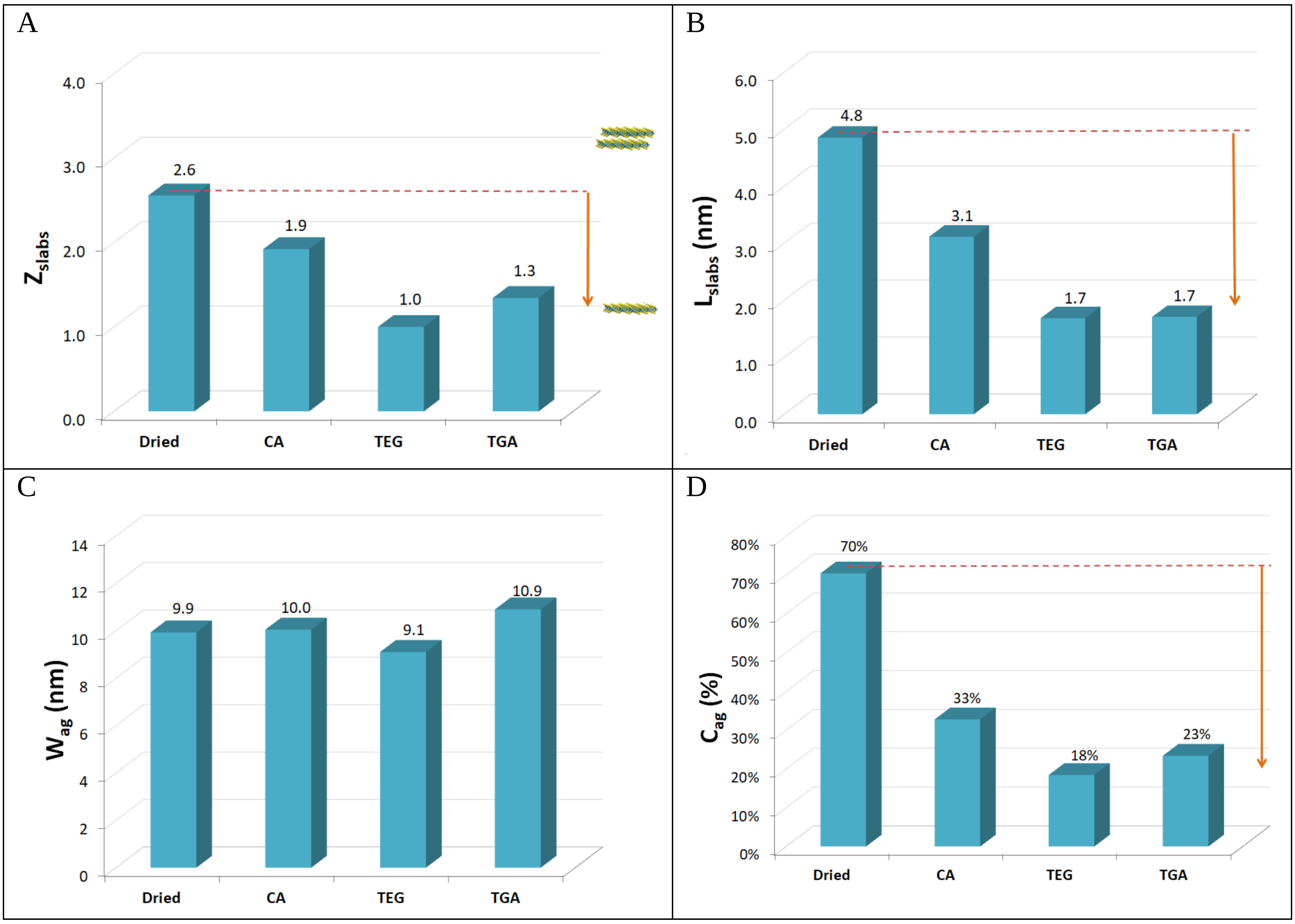

Figure 5. Graphical representation of the slabs stacking z_{slabs} (A), slabs mean length L_{slabs} (B), aggregates mean width W_{ag} (C) and aggregate content C_{ag} (D) parameters for the Dried-liquid, CA-liquid, TEG-liquid, TEG-liquid and TGA-liquid samples.

3.2.2 Effect of the sulfidation condition

Comparing the ASAXS curves obtained on gas sulfide catalysts (Figure 2) and liquid sulfided catalysts (Figure 3), the Mo slab characteristics such as their distribution within the alumina support appear to be different according to the sulfidation conditions. In order to highlight the main differences, the various parameters are compared on Figure 6.

At the individual slab scale (Figure 6 A and B), the additivated catalysts all show the same trends: a gas phase sulfidation, compared to a liquid phase sulfidation, leads to slabs up to twice as long and up to three times more stacked (the z_{slabs} parameter goes from 1 to 3). The stack of gas phase sulfided slabs is particularly visible on the ASAXS curves on Figure 2 with the presence of a correlation peak around 1 Å^{-1}. The same trend is observed by TEM, with an increase of the length of the slabs using the gas sulfidation (Table 2). Similar conclusion has been also derived from EXAFS analysis of the Mo-Mo coordination numbers of the second shell of the MoS_2 nanoslabs [16,54]. Greater coordination numbers are usually reported for sulfide catalysts activated under gas compared to liquid activation and interpreted as the result of larger MoS_2 slabs. However the differences in refined coordination numbers are small and within the experimental error bars making the conclusion more uncertained than the values reported herein. Furthermore, the effect on the slab stacking is not accessible by EXAFS and not obvious by TEM, while it is clearly observed by ASAXS for TEG-sample, even qualitatively on the SAXS curves, which is one of the strengths of this technique compared to local range order technique and TEM.

As discussed before, TEM and ASAXS slab length values are not in a close agreement and once again, it appears that ASAXS analysis allows one to obtain a more detailed and representative description of the slabs when TEM cannot discriminate the different samples.

At the aggregate scale, significant modifications are also observed. First, as seen in Figure 6-D, the aggregate content (C_{ag}) is affected by the type of sulfidation, depending on the presence and the type of additives: on one hand, gas sulfidation leads to lower C_{ag} for the dried-catalyst compared to liquid sulfidation by almost 20%, but on the other hand higher amounts of aggregates for the TEG additivated-catalyst sulfided under gas is reported compared to the one prepared under liquid activation. Less influence is observed on the C_{ag} TGA-sample. It seems that the aggregation phenomenon is not influenced by the use of additives to the same extent depending on the activation. Secondly, gas sulfidation leads to larger slabs aggregates (W_{ag}, as seen in Figure 6-C) with aggregates width up to 13 nm, or even 17 nm for the CA-gas catalyst.

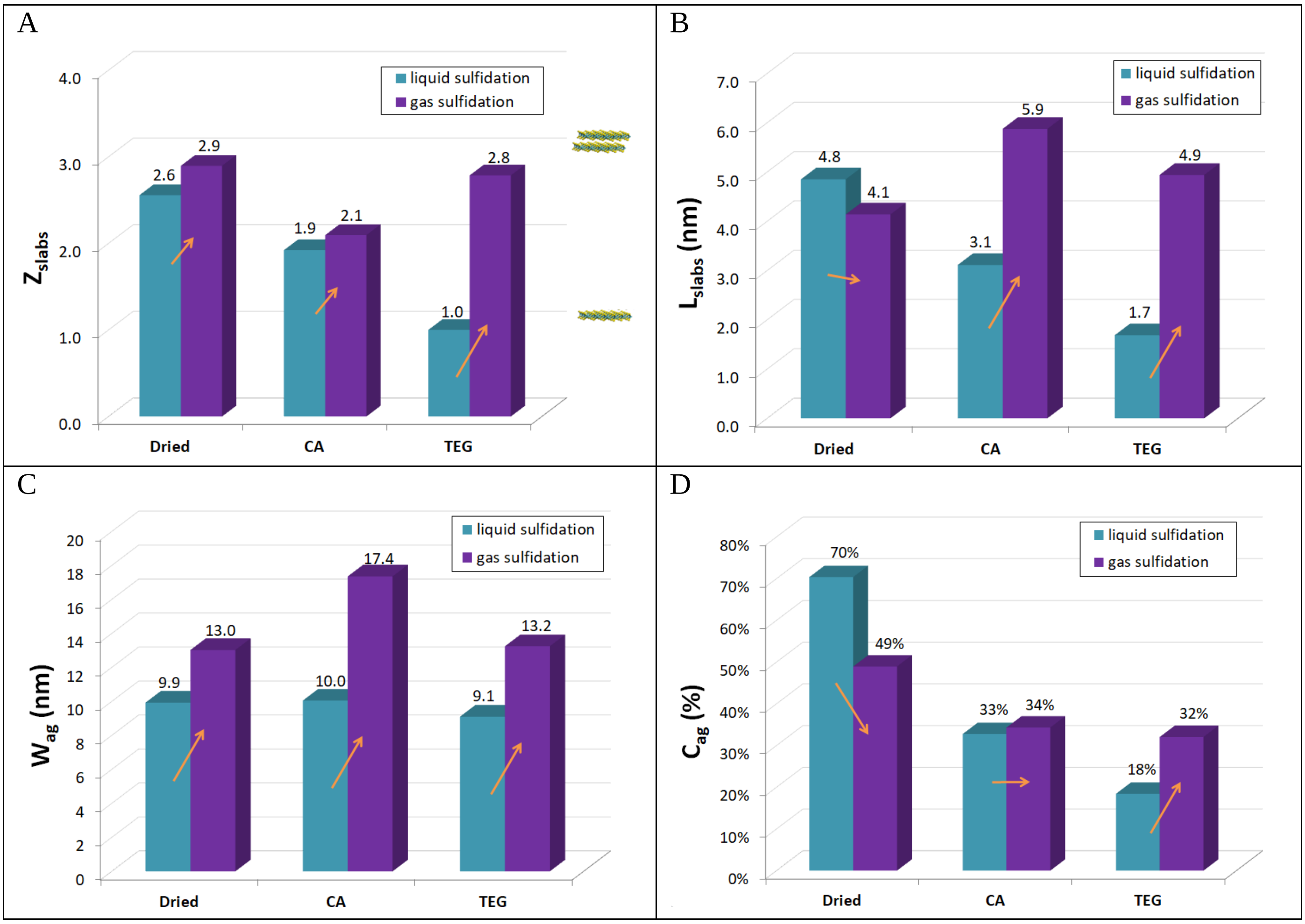

Figure 6. Graphical representation of the slabs stacking z_{slabs} (A), slabs mean length L_{slabs} (B), aggregates mean width W_{ag} (C) and aggregate content C_{ag} (D) parameters as a function of additive and type of sulfidation.

As an indication, TEM image obtained on TEG-gas sample is shown in Figure 7. It highlights the presence of slab aggregates within the sample. The representation remains very local since the image concerns an area of about 60 nm^2 and the quantification of the number of aggregates is impossible at the sample scale. However, this observation shows that the orders of magnitude of the aggregate dimensions obtained by ASAXS are compatible with the objects observed by TEM (between 10 and 60 nm).

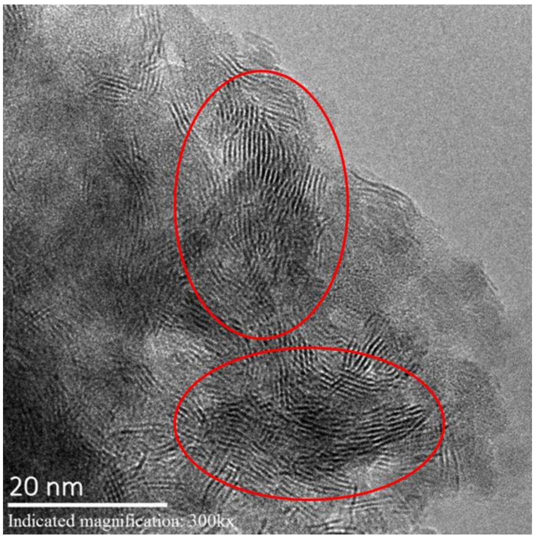

Figure 7. TEM image obtained on the TEG-gas catalyst.

Based on the ASAXS results, it can be concluded that the liquid phase sulfidation has a dispersing effect compared to the gas phase one: the slabs are less stacked and in presence of additives, better distributed within the support (fewer and smaller aggregates). These results are fairly consistent with XPS data: the Mo/Al ratios measured on the gas sulfided catalysts are lower than the ones of the liquid sulfided and additivated catalysts, as reported Table 2, which reveals a lower Mo distribution on the surface. This is also in line with the few studies in the literature comparing both activation ways and showing that liquid sulfidation leads to smaller slabs [10,13–15].

The presence of hydrocarbon molecules during the liquid sulfidation can potentially play a dispersing role. This effect has already been observed in the literature by Glasson et al [55], not by comparing a liquid phase sulfidation and a gas phase sulfidation, but by studying the impact of carbon deposition on thiophene conversion and real feedstock desulfurization activity of sulfided catalysts prepared by gas sulfidation: an oxide catalyst was treated, either by impregnation with C20 gas oil, or by a toluene solution in order to deposit carbon. They showed that the Mo/Al weight ratio measured by XPS increased (from 0.13 to 0.16 approximately) due to carbon deposition, thus revealing a better distribution of MoS_2 slabs.

In addition to the dispersing phenomenon related to the presence of hydrocarbon molecules, the operating conditions specific to liquid sulfidation can also influence the morphology of the active phase. Indeed, during liquid sulfidation, the decomposition of DMDS and the massive release of H_2S occur mainly around 220 °C, contrary to gas-phase sulfidation where H_2S is introduced at room temperature. According to the work of Lesage et al. [16], the sulfidation of Mo during the liquid phase sulfidation of a dried

CoMoP catalyst was shown to generate intermediates MoS_x species of smaller size than in the gas phase which could also explain a better dispersion / distribution of the MoS_2 phase then formed.

3.2.3 Influence of the additives using gas sulfidation

We have seen that for liquid-sulfided catalysts, the three additives had a dispersant effect on the molybdenum: the slabs were smaller, less stacked, and better distributed within the support (fewer and smaller aggregates) compared to the dried catalyst (Figure 5). This behavior is significantly attenuated when sulfided in gas-phase (Table 3). When adding TEG, the slab length and stacking remain nearly unchanged. The slab length is 4.9 for the TEG-gas catalyst, compared to 4.1 nm for the dried-gas sample and the z_{slabs} stacking parameter remains around 2.9. Similarly, the aggregate morphology remains unchanged. However, the effect of TEG is still visible when looking at the aggregate content: it slightly decreases from 49% for the dried catalyst to 32%. Thus, the dispersant effect of TEG is still present, but significantly less efficient in gas-phase sulfidation than in liquid-phase sulfidation.

Besides, citric acid seems to behave differently during gas sulfidation. Indeed, the CA-gas catalyst shows longer slabs (5.9 nm) and spherical aggregates with 18 nm diameter. It can be concluded that CA additive has a different role involving different chemical mechanisms on the Mo active phase formation than the TEG additive. As said previously the role of citric acid as complexing agent of oxidic species has been reported for gas sulfidation as acting more on the improvement of the promotion of MoS_2 [47–51] than on the dispersion [52], as suggested also by the lowest Mo/Al ratio of 0.28 measured by XPS.

The significant differences evidenced by ASAXS in slab and aggregate characteristics depending on the sulfidation conditions point out how the study of the effect of additives with a liquid sulfidation is relevant since this is the sulfidation procedure used industrially. The effects of additives are better evidenced by this type of activation.

3.2.4 Evolution of the catalyst under reaction conditions

The liquid-sulfided catalysts were also analyzed after real feedstock catalytic test. The comparison of the results on the spent catalysts with those gathered before testing, i.e. right after the liquid sulfidation step, allows us to discuss the evolution of the Mo active phase under reaction conditions. Several trends seem to emerge:

At the isolated slab scale (L_{slabs}, z_{slabs}), there is not a single observed behavior. The slab stacking remains relatively stable for calcined, CA, TEG and TGA catalysts, but it slightly decreases for dried-catalyst. The evolution of the slab length is not universal: it tends to decrease for all the catalysts, except for the TEG-sample for which no variation is clearly observed, and for the TGA-catalyst for which slab length increases from 1.7 to 4.7 nm (Table 3).

However the significant evolutions are observed at a larger scale (Figure 10 A and B). For the dried, CA and TEG samples, the aggregate width (W_{ag}) increases of about 3.5 to 6 nm and the aggregate amount (C_{ag}) drastically decreases, suggesting a redispersion of the active phase. At the opposite, the calcined sample remains relatively stable under reaction conditions. Concerning the catalyst prepared with TGA, its behavior is very different: as already mentioned, the slab length increases significantly (from 1.7 to 4.7 nm) and the aggregate amount characterized by a larger width also increases, from 23% to 28%. It suggests a sintering phenomenon of the active phase, in agreement with the decrease of the Mo/Al weight ratio from 0.43 to 0.30, and a high mobility of molybdenum on the support.

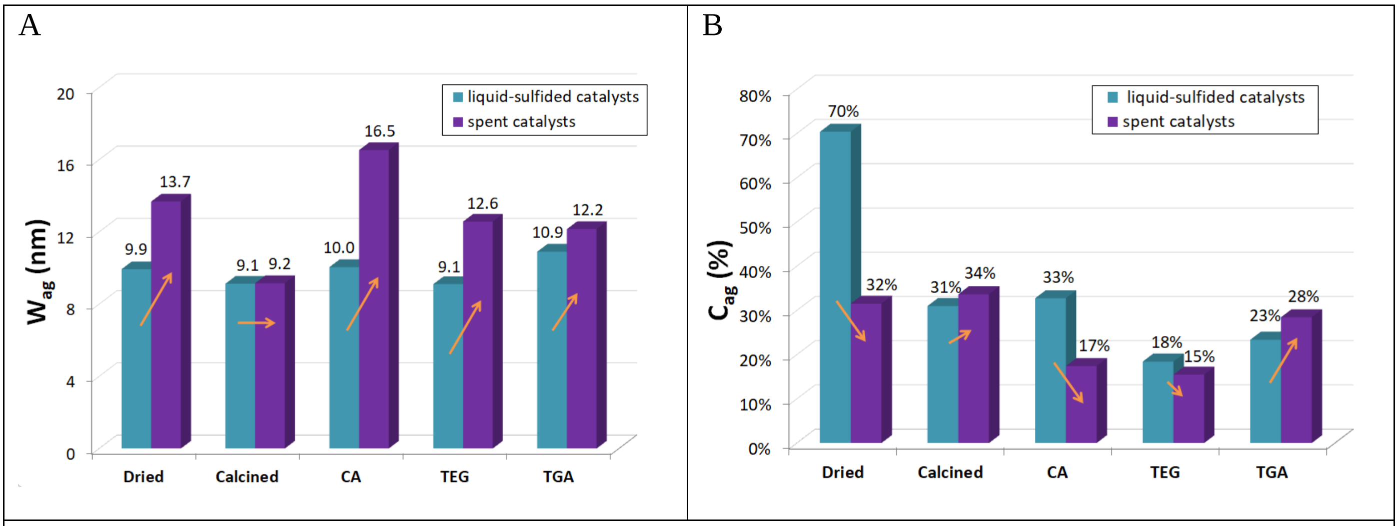

Figure 8. Graphical representation of aggregate mean width W_{ag} (A) and aggregate content C_{ag} (B) parameters for liquid-sulfided catalysts and the spent-catalysts.

These results show clear modification of the Mo distribution and highlight a redispersion or a slab exfoliation during the catalytic test, except for the TGA sample, which may be explained by two mechanisms. First, some small Mo particles may continue to sulfide during the test (supported with the increased % MoS_2 estimated by XPS), increasing the relative amount of isolated slabs (and thus the decrease of the relative amount of aggregate), and decreasing the average slab length. Besides, we can also assume that some aggregates exfoliate or re-disperse, thanks to the presence of the hydrocarbon molecules in the feedstock and the pressure, thus reducing the number of aggregates or increasing the porosity of the aggregates. Indeed, the parameter C_{ag} depends on both Mo content and porosity of the aggregates (see equations 34 and 35). This behavior could explain the increase in the aggregate width. This exfoliation phenomenon has already been mentioned in the literature [56,57], which shows that the stacking of hydrotreating catalyst slabs decreases to 1 after 4 years of industrial hydrotreatment. In addition, the pressure seems to play a role since a decrease in the stacking is observed in the literature when the pressure increases [56,57]. This result has also been observed for catalysts tested in dibenzothiophene [57]. It is then assumed that the stack formation of slabs thanks to the van der Waals forces seems counterbalanced by the strong interaction of adsorbed hydrocarbon molecules, ensuring the stability of single layers of MoS_2.

3.2.5 Conclusion on the Mo dispersion

We have seen that for well-chosen additives, such as triethyleneglycol, better distribution of the Mo slabs within the support is obtained, by reducing the content of slab aggregates. Moreover, a liquid-phase sulfidation also improves this distribution: an exfoliation phenomenon can then be evoked. Finally, under reaction conditions, this phenomenon seems to be ongoing since the aggregate content continues to decrease, but its importance seems to be dependent on the additive used.

3.3 Influence of Mo dispersion on the activity

The relative intrinsic activities (RIA) were first evaluated by a HDS catalytic test on a real feedstock. They are plotted against the C_{ag} parameter (traducing the aggregate content) measured by ASAXS on the fresh liquid-sulfided catalysts (see Figure 9) and then against the aggregate content measured by ASAXS on the spent catalysts (see Figure 10).

No obvious correlation between the activity and the aggregate content measured on the fresh catalysts is observed in Figure 9. However, we have seen before that the morphology of the active phase in the catalysts significantly evolved under reaction conditions. With the activity being measured at the end of the test, it seems more appropriate to study the activity regarding the spent catalyst properties. In this case, as observed in Figure 10, the activity seems better correlated with the aggregate content, with an exception for the calcined catalyst. This trend traduces the significant effect of the Mo dispersion on the catalytic activity: a lower C_{ag} parameter is linked to a higher dispersion of the active phase and to a higher intrinsic activity.

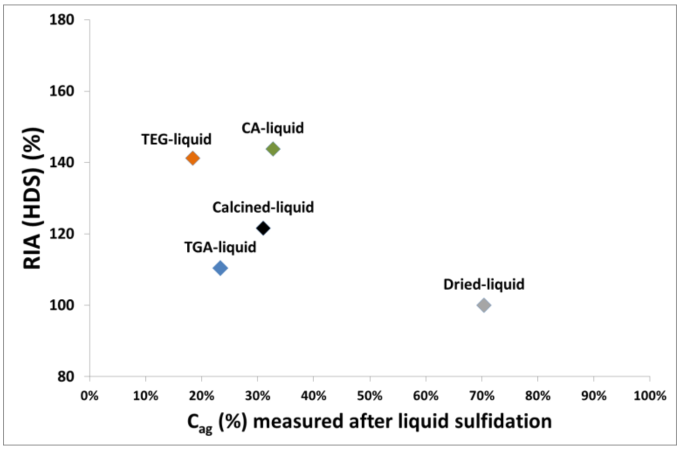

Figure 9. RIA activities measured in HDS test as a function of aggregate content C_{ag} parameter measured on fresh liquid-catalysts.

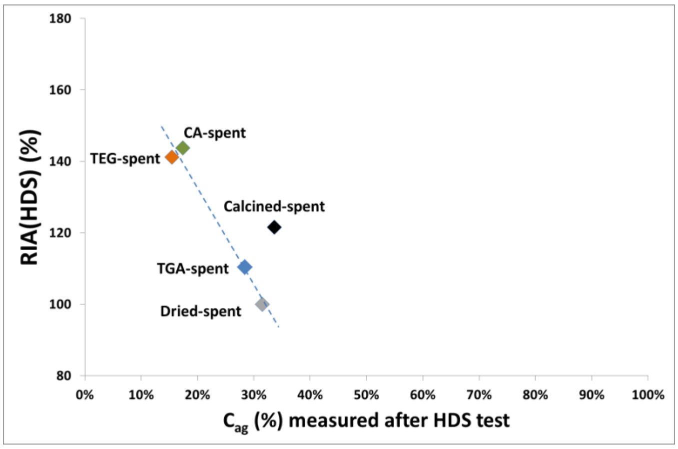

Figure 10. RIA activities measured in HDS test as a function of aggregate content C_{ag} parameter measured on spent-catalysts.

To confirm this trend, the liquid-sulfided catalysts have also been evaluated thanks to a toluene hydrogenation test and the characteristics of the spent catalysts measured by ASAXS.

Once again, when plotting the activity against the aggregate content measured on fresh liquid-sulfided catalysts, no obvious trend is observed (not shown here), whereas the correlation is clearly observed on Figure 11 between the activity for toluene hydrogenation test and the aggregate C_{ag} parameter measured by ASAXS for the spent catalysts. These results make us think that the liquid-sulfided catalysts evolve also during the toluene hydrogenation test, in a comparable manner as in the real HDS test.

To go further, the gas-sulfided catalysts have been also integrated into this activity/dispersion study. The spent gas-sulfided catalysts were not analyzed by ASAXS so we did not get the possibility to confront their activity with the aggregate content of the spent catalysts. However, a good correlation between the aggregate content of the fresh gas-sulfided catalysts and RIA activity is observed (Figure 12). Thus, it can be supposed that the catalyst sulfided in gas-phase conditions at 400°C are more stable under catalytic test conditions than the ones sulfided in liquid-phase conditions and that the physico-chemical properties do not evolve significantly.

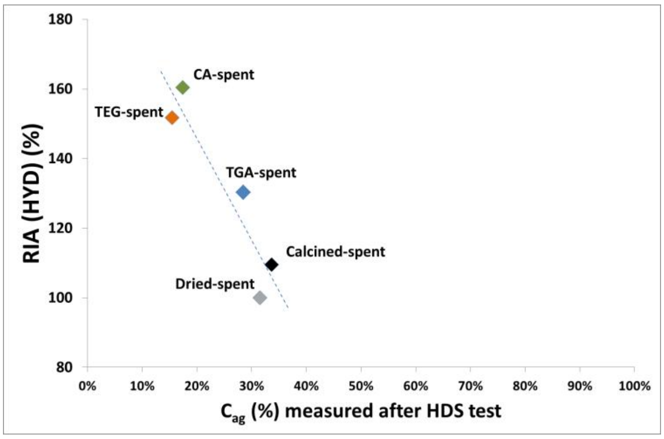

Figure 11. RIA activities measured in toluene hydrogenation test as a function of aggregate content C_{ag} parameter measured on spent-catalysts.

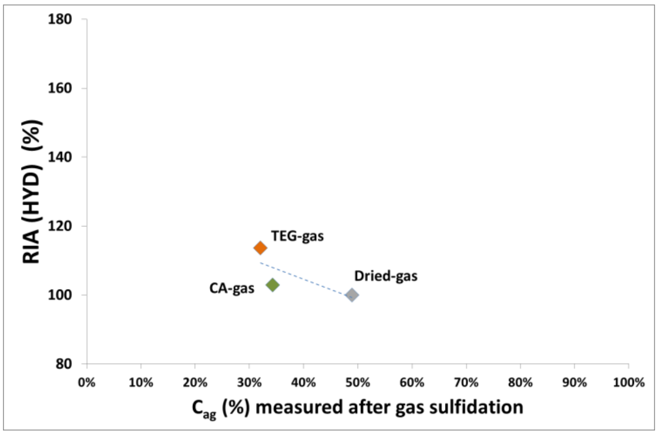

Figure 12. RIA activities measured in toluene hydrogenation test as a function of aggregate content C_{ag} parameter measured on gas-catalysts.

Finally, all these results presented in Figure 11 and Figure 12 were gathered in Figure 13 in order to extract a general trend: the intrinsic activity in toluene hydrogenation is well correlated with the aggregate content and so with the Mo dispersion. Two hypotheses can be formulated to explain the effect of the aggregation state on the activity. Active sites located on the slab edges are probably not entirely accessible inside the aggregates which could limit the global activity of the catalyst. Another explanation is that the aggregates block a part of the porosity, which leads to limit the access of the molecules to the active sites. Deeper studies need to be performed to further understand their effect. Nevertheless, this parameter seems to be crucial in the future development of catalysts. However, it is obviously not sufficient to describe the catalytic activity as the slab length, the sulfidation rate or the promotion rate are also known to be important parameters to control. This graph also highlights the positive effect of TEG and citric acid coupled with liquid sulfidation on the dispersion and thus the activity in line which what has been reported for citric acid by Gonzales-Cortes [53].

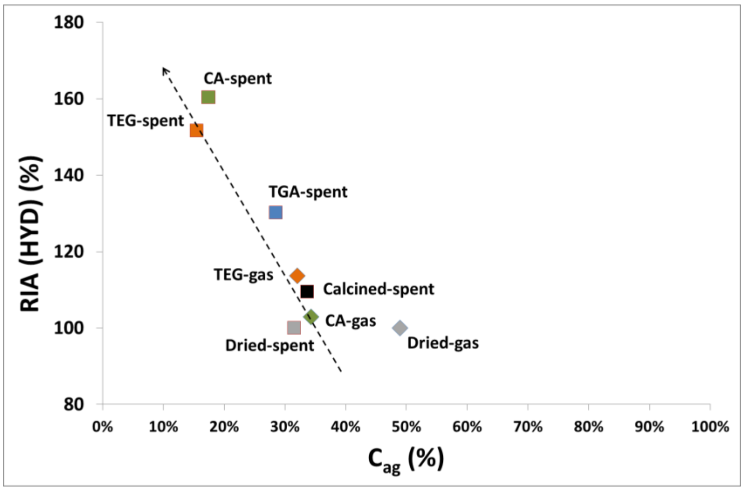

Figure 13. RIA activities in toluene hydrogenation as a function of aggregate content C_{ag} parameter for all catalysts.

4 Conclusion

In this work, we have studied the contribution of the ASAXS technique to the description of the multiscale organization of MoS_2 slabs obtained from different activation routes of additivated CoMoP hydrotreating catalysts.

At the isolated slab scale, ASAXS analysis allows a more detailed and representative description of the slabs compared to TEM which is generally limited to the visualization of a small number of particles bigger than 1 nm. At a larger scale, the technique is unique to identify and quantify the aggregation state of the particles which occurs on high Mo loaded catalysts. We have shown the importance of characterizing the catalysts as close as possible to their industrial conditions when a correlation is sought with their activity since their dispersion (size and stacking of slabs) and aggregation are modified between the gas (laboratory) or liquid (industrial) activation step and after the end of the catalytic test on a real feedstock.

The role of the additives is highlighted after liquid sulfidation activation, as we clearly demonstrate the dispersive effect of TEG and TGA and to a lower extent of citric acid. The slab length and stacking are decreased, as well as the aggregate amount and size. Among other parameters, the aggregate amount appears as a relevant descriptor to correlate the catalytic performances of the studied catalyst, as it will impact the accessibility of the molecules to the active sites. Indeed, the lower the aggregates are, the better the catalytic activity is. This analytical methodology appears to be very relevant for the study of sulfide catalysts, particularly when they have high metals loading. Indeed, we can imagine in the future a deeper understanding of the role of this multiscale slab organization, which is currently too little studied, on the catalytic performances, depending on the support, or under operating conditions of catalytic tests for example.

5 References

[1] C. Song, An overview of new approaches to deep desulfurization for ultra-clean gasoline, diesel fuel and jet fuel, Catalysis Today 86 (2003) 211–263. https://doi.org/10.1016/S0920-5861(03)00412-7.

[2] B. Rebours, R. Revel, A.A. Quoineaud, Characterisation of the Crystal Structure of Aluminas, in: H. Toulhoat, P. Raybaud (Eds.), Catalysis by Transition Metal Sulfides: From Molecular Theory to Industrial Application, Technip, 2013, pp. 376–386.

[3] H. Topsøe, B.S. Clausen, F. Massoth, in: J.R. Anderson, M. Boudart (Ed.), Hydrotreating Catalysis Science and Technology, vol 11, Springer, Berlin Heidelberg, 1996.

[4] D. Laurenti, B. Phung-Ngoc, C. Roukoss, E. Devers, K. Marchand, L. Massin, L. Lemaitre, C. Legens, A.-A. Quoineaud, M. Vrinat, Intrinsic potential of alumina-supported CoMo catalysts in HDS: Comparison between γc, γT, and δ-alumina, JOURNAL OF CATALYSIS 297 (2013) 165–175. https://doi.org/10.1016/j.jcat.2012.10.006.

[5] D. NICOSIA, R. PRINS, The effect of glycol on phosphate-doped CoMo/AlO hydrotreating catalysts, JOURNAL OF CATALYSIS 229 (2005) 424–438. https://doi.org/10.1016/j.jcat.2004.11.014.

[6] E.P. C. Lamonier, Alumina-supported Oxide Precursors Prepared from Heteropolyanions, in: H. Toulhoat, P. Raybaud (Eds.), Catalysis by Transition Metal Sulfides: From Molecular Theory to Industrial Application, Technip, 2013, pp. 151–180.

[7] V. Costa, K. Marchand, M. Digne, C. Geantet, New insights into the role of glycol-based additives in the improvement of hydrotreatment catalyst performances, Catalysis Today 130 (2008) 69–74. https://doi.org/10.1016/j.cattod.2007.05.013.

[8] T.S. Nguyen, S. Loridant, L. Chantal, T. Cholley, C. Geantet, Effect of glycol on the formation of active species and sulfidation mechanism of CoMoP/Al2O3 hydrotreating catalysts, Applied Catalysis B: Environmental 107 (2011) 59–67. https://doi.org/10.1016/j.apcatb.2011.06.037.

[9] J. Escobar, M.C. Barrera, J.A. Toledo, M.A. Cortés-Jácome, C. Angeles-Chávez, S. Núñez, V. Santes, E. Gómez, L. Díaz, E. Romero, J.G. Pacheco, Effect of ethyleneglycol addition on the

properties of P-doped NiMo/Al2O3 HDS catalysts: Part I. Materials preparation and characterization, Applied Catalysis B: Environmental 88 (2009) 564–575. https://doi.org/10.1016/j.apcatb.2008.10.005.

[10] L. van Haandel, G.M. Bremmer, E. Hensen, T. Weber, The effect of organic additives and phosphoric acid on sulfidation and activity of (Co)Mo/Al 2 O 3 hydrodesulfurization catalysts, JOURNAL OF CATALYSIS 351 (2017) 95–106. https://doi.org/10.1016/j.jcat.2017.04.012.

[11] N. Rinaldi, T. Kubota, Y. Okamoto, Effect of citric acid addition on the hydrodesulfurization activity of MoO3/Al2O3 catalysts, Applied Catalysis A: General 374 (2010) 228–236. https://doi.org/10.1016/j.apcata.2009.12.015.

[12] E. Le Guludec, L. Oliviero, J.P. Gilson, F. Maugé, M. Rebeilleau, V. de Grandi, S. van Donk, From Gas to Liquid Phase Sulfidation: An IR Spectroscopy Study, Catalysis Letters 142 (2012) 736–743. https://doi.org/10.1007/s10562-012-0813-5.

[13] P.A. Nikulshin, A.V. Mozhaev, K.I. Maslakov, A.A. Pimerzin, V.M. Kogan, Genesis of HDT catalysts prepared with the use of Co2Mo10HPA and cobalt citrate: Study of their gas and liquid phase sulfidation, Applied Catalysis B: Environmental 158-159 (2014) 161–174. https://doi.org/10.1016/j.apcatb.2014.04.013.

[14] S. Eijsbouts, L.C.A. van den Oetelaar, J.N. Louwen, R.R. van Puijenbroek, G.C. van Leerdam, Changes of MoS 2 Morphology and the Degree of Co Segregation during the Sulfidation and Deactivation of Commercial Co−Mo/Al 2 O 3 Hydroprocessing Catalysts, Ind. Eng. Chem. Res. 46 (2007) 3945–3954. https://doi.org/10.1021/ie061131x.

[15] N. Frizi, P. Blanchard, E. Payen, P. Baranek, M. Rebeilleau, C. Dupuy, J.P. Dath, Genesis of new HDS catalysts through a careful control of the sulfidation of both Co and Mo atoms: Study of their activation under gas phase, Catalysis Today 130 (2008) 272–282. https://doi.org/10.1016/j.cattod.2007.10.109.

[16] C. Lesage, E. Devers, C. Legens, G. Fernandes, O. Roudenko, V. Briois, High pressure cell for edge jumping X-ray absorption spectroscopy, Catalysis Today 336 (2019) 63–73. https://doi.org/10.1016/j.cattod.2019.01.081.

[17] P. Munnik, P.E. de Jongh, K.P. de Jong, Control and Impact of the Nanoscale Distribution of Supported Cobalt Particles Used in Fischer-Tropsch Catalysis, Journal of the American Chemical Society 136 (2014) 7333–7340. https://doi.org/10.1021/ja500436y.

[18] P. Munnik, N.A. Krans, P.E. de Jongh, K.P. de Jong, Effects of Drying Conditions on the Synthesis of Co/SiO2 and Co/Al2O3 Fischer–Tropsch Catalysts, ACS Catalysis 4 (2014) 3219–3226. https://doi.org/10.1021/cs5006772.

[19] S. Humbert, G. Desjouis, T. Bizien, L. Lemaitre, A.L. Taleb, C. Dalverny, L. Sorbier, A.S. Gay, Effect of reduction on Co catalyst active phase highlighted by an original approach coupling ASAXS and electron tomography, JOURNAL OF CATALYSIS 366 (2018) 202–212. https://doi.org/10.1016/j.jcat.2018.07.024.

[20] L. Zavala-Sanchez, X. Portier, F. Maugé, L. Oliviero, High-resolution STEM-HAADF microscopy on a γ-Al2O3 supported MoS2 catalyst—proof of the changes in dispersion and morphology of the slabs with the addition of citric acid, Nanotechnology 31 (2019) 35706. https://doi.org/10.1088/1361-6528/ab483c.

[21] G. Beaucage, H.K. Kammler, S.E. Pratsinis, Particle size distributions from small-angle scattering using global scattering functions, J. Appl. Crystallogr. 37 (2004) 523–535. https://doi.org/10.1107/s0021889804008969.

[22] H.K. Kammler, G. Beaucage, R. Mueller, S.E. Pratsinis, Structure of Flame-Made Silica Nanoparticles by Ultra-Small-Angle X-ray Scattering, Langmuir 20 (2004) 1915–1921. https://doi.org/10.1021/la030155v.

[23] S. Polizzi, P. Riello, G. Goerigk, A. Benedetti, Quantitative investigations of supported metal catalysts by ASAXS, Journal of Synchrotron Radiation 9 (2002) 65–70. https://doi.org/10.1107/s0909049502000948.

[24] H.G. Haubold, T. Vad, N. Waldofner, H. Bonnemann, From Pt molecules to nanoparticles, J. Appl. Crystallogr. 36 (2003) 617–620. https://doi.org/10.1107/s0021889803005144.

[25] H.G. Haubold, X.H. Wang, ASAXS studies of carbon-supported electroctalysts, Nuclear Instruments & Methods in Physics Research Section B-Beam Interactions with Materials and Atoms 97 (1995) 50–54.

[26] H.G. Haubold, X.H. Wang, G. Goerigk, W. Schilling, In situ anomalous small-angle X-ray scattering investigation of carbon-supported electrocatalysts, J. Appl. Crystallogr. 30 (1997) 653–658. https://doi.org/10.1107/s0021889897002422.

[27] H.G. Haubold, X.H. Wang, H. Jungbluth, G. Goerigk, W. Schilling, In situ anomalous small-angle X-ray scattering and X-ray absorption near-edge structure investigation of catalyst structures and reactions, Journal of Molecular Structure 383 (1996) 283–289.

[28] A. Benedetti, Small-angle scattering of heterogeneous catalysts, J. Appl. Crystallogr. 30 (1997) 647–652.

[29] S. Ciccariello, A. Benedetti, F. Pinna, G. Strukul, W. Juszczyk, H. Brumberger, X-Ray study of metallic particle sintering in Pt-NaY zeolite catalysts, Physical Chemistry Chemical Physics 1 (1999) 367–372.

[30] T. Binninger, M. Garganourakis, J. Han, A. Patru, E. Fabbri, O. Sereda, R. Kötz, A. Menzel, T.J. Schmidt, Particle-Support Interferences in Small-Angle X-Ray Scattering from Supported-Catalyst Materials, Phys. Rev. Applied 3 (2015). https://doi.org/10.1103/PhysRevApplied.3.024012.

[31] L. Haandel, A. Longo, W. Bras, E.J.M. Hensen, T. Weber, Activation of Co−Mo−S Hydrodesulfurization Catalysts Under Refinery Conditions-A Combined SAXS/XAS Study, ChemCatChem 11 (2019) 5013–5017. https://doi.org/10.1002/cctc.201901390.

[32] N. Frizi, P. Blanchard, E. Payen, P. Baranek, C. Lancelot, M. Rebeilleau, C. Dupuy, J.P. Dath, Genesis of new gas oil HDS catalysts: Study of their liquid phase sulfidation, Catalysis Today 130 (2008) 32–40. https://doi.org/10.1016/j.cattod.2007.10.008.

[33] S. Texier, G. Berhault, G. Pérot, F. Diehl, Activation of alumina-supported hydrotreating catalysts by organosulfides or H2S, Applied Catalysis A: General 293 (2005) 105–119. https://doi.org/10.1016/j.apcata.2005.07.026.

[34] A. Vonortas, N. Papayannakos, Kinetic Study of the Hydrodesulfurization of a Heavy Gasoil in the Presence of Free Fatty Acids Using a CoMo/γ-Al 2 O 3 Catalyst, Ind. Eng. Chem. Res. 53 (2014) 9646–9652. https://doi.org/10.1021/ie5006492.

[35] G.A. Chahine, N. Blanc, S. Arnaud, F. de Geuser, R. Guinebretière, N. Boudet, Advanced Non-Destructive in Situ Characterization of Metals with the French Collaborating Research Group D2AM/BM02 Beamline at the European Synchrotron Radiation Facility, Metals 9 (2019) 352. https://doi.org/10.3390/met9030352.

[36] F. Zhang, J. Ilavsky, G.G. Long, J.P.G. Quintana, A.J. Allen, P.R. Jemian, Glassy Carbon as an Absolute Intensity Calibration Standard for Small-Angle Scattering, Metallurgical and Materials Transactions A 41 (2010) 1151–1158. https://doi.org/10.1007/s11661-009-9950-x.

[37] A.C. Thompson, X-Ray Data Booklet, Berkeley, C.A: Lawrence Berkeley National Laboratory, 2009.

[38] C.T. Chantler, Theoretical Form Factor, Attenuation, and Scattering Tabulation for Z=1–92 from E=1–10 eV to E=0.4–1.0 MeV, Journal of Physical and Chemical Reference Data 24 (1995) 71–643. https://doi.org/10.1063/1.555974.

[39] C.T. Chantler, Detailed Tabulation of Atomic Form Factors, Photoelectric Absorption and Scattering Cross Section, and Mass Attenuation Coefficients in the Vicinity of Absorption Edges in the Soft X-Ray (Z=30–36, Z=60–89, E=0.1 keV–10 keV), Addressing Convergence Issues of Earlier Work, J. Phys. Chem. Ref. Data 29 (2000) 597. https://doi.org/10.1063/1.1321055.

[40] F. Wen, N. Waldofner, W. Schmidt, K. Angermund, H. Bonnemann, S. Modrow, S. Zinoveva, H. Modrow, J. Hormes, L. Beuermann, S. Rudenkiy, W. Maus-Friedrichs, V. Kempter, T. Vad, H.G.

Haubold, Formation and characterization of Pt nanoparticle networks, European Journal of Inorganic Chemistry (2005) 3625–3640. https://doi.org/10.1002/ejic.200500446.

[41] M. Sztucki, E. Di Cola, T. Narayanan, New opportunities for Anomalous Small-Angle X-Ray Scattering to characterize Charged Soft Matter Systems, in: A. Takahara, K. Sakurai (Eds.), Future trends in soft materials research with advanced light sources, 2011.

[42] M. Sztucki, E. Di Cola, T. Narayanan, Instrumental developments for anomalous small-angle X-ray scattering from soft matter systems, Journal of Applied Crystallography 43 (2010) 1479–1487. https://doi.org/10.1107/S002188981003298X.

[43] H.B. Stuhrmann, Resonance scattering in macromolecular structure research, in: H.H. Kausch, H.G. Zachmann (Eds.), Characterization of Polymers in the Solid State II: Synchrotron Radiation, X-ray Scattering and Electron Microscopy, Springer Berlin Heidelberg, Berlin, Heidelberg, 1985, pp. 123–163.

[44] S. Haas, A. Hoell, G. Zehl, I. Dorbandt, P. Bogdanoff, S. Fiechter, Structural Investigation of Carbon Supported Ru-Se Based Catalysts using Anomalous Small Angle X-Ray Scattering, ECS Transac 6 (2008). https://doi.org/10.1149/1.2943231.

[45] E.S. Kadantsev, P. Hawrylak, Electronic structure of a single MoS2 monolayer, Solid State Communications 152 (2012) 909–913. https://doi.org/10.1016/j.ssc.2012.02.005.

[46] A.L. Nuzhdin, G.A. Bukhtiyarova, P.E. Plyusnin, A.A. Porsin, V.I. Bukhtiyarov, Effect of Mono-, Di-, and Triethylene Glycol on the Sulfidation Behavior of NiMo(P)/Al2O3 Hydrotreating Catalysts, Catal Lett 149 (2019) 3304–3311. https://doi.org/10.1007/s10562-019-02898-1.

[47] P. Castillo-Villalón, J. Ramirez, J.A. Vargas-Luciano, Analysis of the role of citric acid in the preparation of highly active HDS catalysts, JOURNAL OF CATALYSIS 320 (2014) 127–136. https://doi.org/10.1016/j.jcat.2014.09.021.

[48] T. Fujikawa, Kato Masahiro, Takeshi Ebihara, Kazuhiko Hagiwara, Takeshi Kubota, Yasuaki Okamoto, Development of highly active Co-Mo catalysts with phosphorus and citric acid for ultra-deep desulfurization of diesel fractions (Part 2) characterization of active sites, journal of the Japan Petroleum Institute 48 (2005) 114–120.

[49] O.V. Klimov, A.V. Pashigreva, M.A. Fedotov, D.I. Kochubey, Y.A. Chesalov, G.A. Bukhtiyarova, A.S. Noskov, Co–Mo catalysts for ultra-deep HDS of diesel fuels prepared via synthesis of bimetallic surface compounds, Journal of Molecular Catalysis A: Chemical 322 (2010) 80–89. https://doi.org/10.1016/j.molcata.2010.02.020.

[50] T. Kubota, N. Rinaldi, K. Okumura, T. Honma, S. Hirayama, Y. Okamoto, In situ XAFS study of the sulfidation of Co–Mo/B2O3/Al2O3 hydrodesulfurization catalysts prepared by using citric acid as a

chelating agent, Applied Catalysis A: General 373 (2010) 214–221. https://doi.org/10.1016/j.apcata.2009.11.023.

[51] J. Chen, J. Mi, K. Li, X. Wang, E. Dominguez Garcia, Y. Cao, L. Jiang, L. Oliviero, F. Maugé, Role of Citric Acid in Preparing Highly Active CoMo/Al 2 O 3 Catalyst, Ind. Eng. Chem. Res. 56 (2017) 14172–14181. https://doi.org/10.1021/acs.iecr.7b02877.

[52] A. Pimerzin, A. Mozhaev, A. Varakin, K. Maslakov, P. Nikulshin, Comparison of citric acid and glycol effects on the state of active phase species and catalytic properties of CoPMo/Al2O3 hydrotreating catalysts, Applied Catalysis B: Environmental 205 (2017) 93–103. https://doi.org/10.1016/j.apcatb.2016.12.022.

[53] S.L. González-Cortés, Y. Qian, H.A. Almegren, T. Xiao, V.L. Kuznetsov, P.P. Edwards, Citric acid-assisted synthesis of γ-alumina-supported high loading CoMo sulfide catalysts for the hydrodesulfurization (HDS) and hydrodenitrogenation (HDN) reactions, Appl Petrochem Res 5 (2015) 181–197. https://doi.org/10.1007/s13203-015-0097-y.

[54] L. van Haandel, G.M. Bremmer, E. Hensen, T. Weber, Influence of sulfiding agent and pressure on structure and performance of CoMo/Al2O3 hydrodesulfurization catalysts, JOURNAL OF CATALYSIS 342 (2016) 27–39. https://doi.org/10.1016/j.jcat.2016.07.009.

[55] C. Glasson, C. Geantet, M. Lacroix, F. Labruyere, P. Dufresne, Beneficial Effect of Carbon on Hydrotreating Catalysts, JOURNAL OF CATALYSIS 212 (2002) 76–85. https://doi.org/10.1006/jcat.2002.3781.

[56] R.R. Chianelli, M.H. Siadati, De la Rosa, M. P., G. Berhault, J.P. Wilcoxon, R. Bearden, B.L. Abrams, Catalytic properties of single layers of transition metal sulfide catalytic materials, Catalysis Reviews-Science and Engineering 48 (2006) 1–41. https://doi.org/10.1080/01614940500439776.

[57] De la Rosa, Myriam Perez, S. Texier, G. Berhault, A. Camacho, M.J. Yácaman, A. Mehta, S. Fuentes, J.A. Montoya, F. Murrieta, R.R. Chianelli, Structural studies of catalytically stabilized model and industrial-supported hydrodesulfurization catalysts, JOURNAL OF CATALYSIS 225 (2004) 288–299. https://doi.org/10.1016/j.jcat.2004.03.039.